Understanding condensation domain selectivity in non-ribosomal peptide biosynthesis: structural characterization of the acceptor bound state

Max Cryle (max.cryle@monash.edu)
Monash University https://orcid.org/0000-0002-9739-6157

Thierry Izore
Monash University

Y. T. Ho
Monash University

Joe Kaczmarski
Australian National University https://orcid.org/0000-0001-8549-0122

Athina Gavriilidou
University of Tuebingen

Ka Chow
University of Queensland

David Steer
Monash University

Robert Goode
Monash University https://orcid.org/0000-0002-3028-8928

Ralf Schittenhelm
Monash University https://orcid.org/0000-0001-8738-1878

Julien Tailhades
Monash University

Manuela Tosin
University of Warwick

Gregory Challis
University of Warwick https://orcid.org/0000-0001-5976-3545

Elizabeth Krenske
The University of Queensland https://orcid.org/0000-0003-1911-0501

Nadine Ziemert
University of Tübingen https://orcid.org/0000-0002-7264-1857

Colin Jackson
Australian National University https://orcid.org/0000-0001-6150-3822

Article

Keywords: Complex Peptide Natural Products, Multi-modular Assembly Lines, Chain Assembly, Acceptor Substrates

Posted Date: January 6th, 2021

DOI: https://doi.org/10.21203/rs.3.rs-125509/v1

Version of Record: A version of this preprint was published at Nature Communications on May 4th, 2021. See the published version at https://doi.org/10.1038/s41467-021-22623-0.

Abstract

Non-ribosomal peptide synthetases are important enzymes for the assembly of complex peptide natural products. Within these multi-modular assembly lines, condensation domains perform the central function of chain assembly, typically by forming a peptide bond between two peptidyl carrier protein (PCP)-bound substrates. In this work, we report the first structural snapshots of a condensation domain in complex with an aminoacyl-PCP acceptor substrate. These structures allow the identification of a mechanism that controls access of acceptor substrates to the active site in condensation domains. The structures of this previously uncharacterized complex also allow us to demonstrate that condensation domain active sites do not contain a distinct pocket to select the side chain of the acceptor substrate during peptide assembly but that residues within the active site motif can instead serve to tune the selectivity of these central biosynthetic domains.

Introduction

Non-ribosomal peptide synthetases (NRPSs) are important biosynthetic enzymes for the production of highly diverse and extensively modified peptides.[1] The diversity of non-ribosomal peptides is due to the combination of an ability to incorporate an expanded range of monomers compared to ribosomal peptide biosynthesis together with extensive modifications of the peptide both during and after chain assembly.[2] This is enabled by the modular architecture of NRPSs, which use repeating groups of catalytic domains to install one monomer into the growing peptide (Fig. 1A). Within a minimal chain extension module, an adenylation (A) domain performs the selection and activation of amino acid building blocks at the expense of ATP, prior to the loading of the monomer onto the phosphopantetheinyl (PPant) moiety of an adjacent peptidyl carrier protein (PCP) domain.[1] Chain assembly is then performed by condensation (C) domains, which typically accept two PCP-bound substrates and catalyze peptide bond formation through the attack of the downstream acceptor substrate upon the thioester of the upstream donor substrate (Fig. 1B).[3] The first X-ray crystal structure of an NRPS C domain (VibH from the vibriobactin NRPS, Fig. 1C)[4] showed that they comprise a pseudo-dimer of the chloramphenicol acetyl transferase (CAT) enzyme fold, with key catalytic residues forming a conserved HHxxxDG motif located at the interface between the two subdomains. In addition, it was shown that C domains harbor two catalytic tunnels that lead from the donor-PCP and acceptor-PCP domain docking sites to the active site and represent the access route for the donor and the acceptor substrates, respectively. This architecture has since been confirmed by other structures.[4–16] While the conserved central histidine (H**H**xxxDG) is generally thought to act as the primary catalytic residue that promotes deprotonation of the α-amino group in the acceptor aminoacyl-PCP as it attacks the thioester, this remains a matter of debate.[3] Perhaps more importantly, the role C domains play in determining NRPS specificity is unclear, in part due to the lack of structural characterization of relevant PCP-bound C domain complexes.

Whilst the modular architecture of NRPSs has attracted great interest from the perspective of biosynthetic engineering,[17–19] such efforts have not always been successful. This can be attributed to the complexity

of the machinery combined with the necessity for non-native substrates to pass through multiple catalytic domains, each of which imparts a degree of specificity. A pertinent example of this is the recent recognition of the diverse functions of C domains in peptide biosynthesis, extending their well-established role in controlling peptide stereochemistry (working in concert with epimerization (E) domains) to gating *in trans* modifications, recruiting *trans*-acting enzymes and performing additional chemical transformations of their substrates during peptide bond formation (Fig. 1C).[20–24] Whilst A domains are the main origin of structural diversity in non-ribosomal peptides,[25] C domains play a key role in peptide bond formation and make important contributions to structural diversification in many valuable compound classes. Thus, gaining a deeper understanding of their function a high priority.

The structural analysis of key domains, complexes and complete modules has made major contributions to our understanding of how selectivity is achieved by NRPS assembly lines.[26] Whilst the structures of isolated modules are incredibly informative, NRPSs are highly flexible[7,13,27,28] and the interactions between individual domains change during the process of chain assembly. Structural characterization of key domain–domain complexes is thus an important goal to improve our understanding of NRPS selectivity. For example, structures of A domains in complex with PCP domains in distinct states, corresponding to substrate binding, substrate activation and PPant loading have provided insight into the mechanisms underlying A domain selectivity [10,29]. However, C domains and C domain-containing complexes have proved more challenging to structurally characterize, with fewer examples reported to date (Fig. 1C).[3,26] Furthermore, no structures of a C domain in complex with an acceptor PCP-domain bearing a substrate have been reported, which makes understanding the origins of C domain specificity for their acceptor substrates unclear, and also limits our understanding of the role of active site residues in C domain catalysis.[3]

To address this, we report the structure and biochemical characterization of complexes of a PCP domain bearing a stable analogue of the acyl acceptor complexed to the acceptor site of a C domain from the NRPS that biosynthesizes fuscachelin in the thermophile *Thermobifida fusca* (Fig. 1A).[30] This structure reveals that the interface between the PCP and C domains is dominated by hydrophobic interactions and that access to the C domain active site is gated by an arginine residue that prevents unloaded PCP-substrates from accessing the active site of the C domain. The C domain is shown to be tolerant of a range of aliphatic acceptor amino acid acceptor substrates, with the limited acceptance of other substrates rationalized through interactions with key residues within the C domain active site. We demonstrate that C domains do not appear to contain an “A domain-like” side chain selectivity pocket to control their acceptor substrates and resolve how substrates engage with central catalytic residues in C domains, both of which are key unanswered questions central to NRPS-mediated peptide biosynthesis.

Results

Structure of the PCP $_2$ -C $_3$ didomain. To elucidate the structure of C domain with a PCP domain bound in the acceptor site, we screened several systems including a thermophilic example of a PCP_2-C_3 didomain

(containing the PCP domain from module 2 and the C domain from module 3) of the fuscachelin NRPS from the thermophilic organism *Thermobifida fusca* (Fig. 1A [red rectangle]).[30] Expression of the fuscachelin PCP_2-C_3 didomain in *E. coli* yielded 0.8 mg/ L of culture of stable protein and afforded crystals that grew rapidly in 18–22% *w/v* PEG 3350 and 0.17–0.3 M magnesium formate at room temperature. Crystals were harvested, cryoprotected in 20–30% glycerol and diffraction data collected at the Australian Synchrotron, with initial phases obtained from a single anomalous diffraction experiment (SAD) using xenon-derivatised crystals (see Methods). The crystals belonged to the $P2_12_12_1$ space group, with the unit cell comprising two highly similar copies of the PCP_2-C_3 construct (RMSD (all atoms) 0.74 Å).

The PCP_2-C_3 didomain structure we obtained from these experiments was solved at a resolution of 2.2 Å (Fig. 2A, **SI Table S1**). When considered separately, the overall folds of both the PCP_2 domain and C_3 domain were consistent with previously reported structures.[26] The PCP_2 domain comprises a 4-helix bundle with a small α-turn between helices 1 and 2 (seen in most crystal structures but absent from NMR structures); the serine residue that is the site of 4'-phosphopantetheine (PPant) attachment is located at the start of helix 2 (Fig. 2B). Of the published crystal structures of PCP domains, this structure is most similar to the PCP domain found in the PCP-Te/R didomain NRPS construct from the archaeon *Methanobrevibacter ruminantium* M1 (PDB ID 6VTJ; RMSD (all atoms) 1.3 Å, 32% sequence similarity, see **SI Table S2**). The C_3 domain of the didomain resembles other members of its class (see **SI Table S3**), comprising a pseudo-dimer of CAT domains with bridge (R2923 to T2944) and floor loop (A2843 to L2858) regions (Figs. 1C & 2C). The catalytic residues sit at the core of the C_3 domain and can be accessed from the bulk solvent via tunnels formed along the interface of the two pseudo-domains (Fig. 2D). Differences in the relative position of these two halves are observed in structures of C domain homologs and can alter the size and character of the acceptor and donor catalytic tunnels.[3] A superimposition of the fuscachelin C_3 domain with two well-characterized C domains (from surfactin and linear gramicidin NRPSs)[7,12] highlights this, with a pronounced difference in displacements observed when comparing the fuscachelin C_3 domain and Srf-A domain (**SI Figure S1**). This aspect of C-domain conformational flexibility and diversity is currently not broadly understood, although recent efforts have been made to understand these conformational differences in terms of the accessibility of the substrates to the active site the C-domain.[9]

In the PCP_2-C_3 didomain structure, the PCP_2 domain sits at the acceptor-PCP binding site (near the opening of the acceptor substrate channel) on the C_3 domain from the second chain in the asymmetric unit. The interface between the PCP_2 domain and C_3 domain is mostly hydrophobic in nature (537/510 $Å^2$ buried surface area (chain A/B) excluding PPant), with the side chains of V2534, L2515, L2518, F2508 and F2538 of the PCP domain playing a major role in the interaction along with residues A2907, V2908, V2584, L2580 and W2579 in the C domain (Fig. 2E, **SI Tables S4-5**). This interface is reminiscent of the hydrophobic interaction pattern described in other structures of PCP domains docked at the acceptor site of C domains (SrfA-C (PDB ID 2VSQ),[12] AB3403 (PDB ID 4ZXH);[10] see also [26]). These interfaces center

around a hydrophobic residue (L2515) immediately following the serine to which the PPant is attached (S2514) and at least one hydrophobic residue ~ 20 amino-acids after the serine residue. R2906 also plays an important role in positioning the docked PCP domain *via* interactions with the phosphate moiety of the PPant arm. In the PCP_2-C_3 structure, these residues are V2534 and the aliphatic moiety of R2535 that interacts with V2908 of the C domain. The overall orientation of the PCP domain relative to the C domain is similar to what has been observed in the structures of SrfA-C [12] and ObiF1 (PDB ID 6N8E)[8] (**SI Figure S2A-B**), whilst other structures contain a PCP domain that is rotated by several degrees around the conserved serine (AB3403,[10] LgrA (PDB ID 6MFZ)[7]) (**SI** Fig. 2C-D). Although the overall orientation of these PCP domains in relation to the C domain are different, it is important to note that the position of the PPant-modified serine (located at the beginning of the second helix) is always maintained at the entrance of the acceptor substrate channel of the C domain.

Since the PCP_2 domain precedes the C_3 domain in the fusachelin NRPS, we had expected that the PCP_2 domain would dock at the donor-PCP binding site of the C_3 domain. We were surprised, therefore, to find that this construct crystallized with the PCP_2 domain docked into the acceptor-PCP binding site of a symmetry-related C_3 domain (Fig. 2A). Given that the PCP_2 and PCP_3 domains of the fuscachelin NRPS are highly similar (65% sequence identity, Fig. 3), and that PCP domains can act as both aminoacyl donors and acceptors for C domains, we rationalized that the arrangement observed in our structure is a valid model of an acceptor-PCP-bound C domain. Indeed, when we determined the structure of the isolated PCP_3 domain, we found its structure to be highly similar to the PCP_2 domain (RMSD (all atoms) 2 Å; Fig. 3A-C). Importantly, the residues at the interface with the C domain are conserved or highly similar (Fig. 3D). Furthermore, computational docking of the PCP_3 domain onto the acceptor-PCP binding site of the C_3 domain showed that it binds in an almost identical orientation to the PCP_2 domain in the structure of the PCP_2-C_3 didomain (**SI Figure S4**). This supports the notion that the PCP_2-C_3 didomain structure is a valid representation of an acceptor-PCP-bound C-domain.

Analysis of the PCP_2-C_3 didomain structure revealed extra density extending from the conserved Ser (S2514) at the beginning of helix 2 of the PCP domain. This serine residue is the target of phosphopantetheinyl transferases, a class of enzymes that attach the essential PPant moiety to PCP domains. Mass spectrometric analysis of the PCP_2-C_3 didomain construct revealed a 340 Dalton mass increase, consistent with attachment of PPant to S2514, likely installed by the phosphopantetheinyl transferase EntD that phosphopantetheinylates some PCP domains when they are expressed in *E. coli*. Indeed, expression of the PCP_2-C_3 didomain construct in an *entD* mutant[31] showed no increase in mass, supporting this hypothesis. Having confirmed the presence of a PPant arm, we modeled this into the electron density observed in our structure. Interestingly, we found that this did not extend into the active site of the C domain, but instead curled back towards the outer surface of the C domain (Fig. 4A). The side chain of R2577 appears to block the channel that leads to the active site of the C domain (Fig. 4A). Molecular dynamics simulations initiated from structures of the C_3 domain (with the PCP-PPant removed) highlight the intrinsically dynamic nature of the acceptor substrate channel and the important

role that R2577 has in modulating its shape and size (**SI Figure S5**). This residue forms the bottleneck of the channel and samples alternate rotamers (primarily rotation around chi-3) that, in concert with a displacement of alpha-helix 1, largely determines its size. When we compared our PCP_2-C_3 didomain structure with published structures of other C domains in complex with a PPant-modified PCP domain, we found residues with shorter side chains at this position (G21 in AB3403[10] and A18 in ObiF1[8]), resulting in channels that do not block PPant access. Interestingly, this Arg residue appears largely conserved in $^{L}C_{L}$ [1] domains (73% harbor an Arg at this position), but is not seen in $^{D}C_{L}$ domains (Gly (80%) or Ala (4%) are found instead (**SI Figure S6**)). Whilst it was unclear what role this residue plays in NRPS function, we hypothesized that it could influence access to acceptor channel of the C domain.

Effect of R2577G mutation on substrate position. To verify the role of the R2577 in controlling access to the catalytic channel, we generated the Arg to Gly mutant (R2577G) of the C_3 domain. To control the modification state of the PCP_2 domain, the mutant PCP_2-C_3 didomain construct was expressed in the *entD* mutant of *E. coli*.[31] After purification, the protein was modified using the promiscuous PPant transferase Sfp R4-4 mutant[32] and coenzyme A (CoA) (See Methods) to ensure homogeneous PPant loading. Similar to the wild type construct, the protein expressed well and crystallized in the same conditions. Crystals diffracted to 2 Å and the structure was phased using molecular replacement with the previous model (**SI Table S1**). The structure of the R2577G mutant is very similar to that of the wild type protein, with the PCP_2 domain sitting at the acceptor site of the C_3 domain (RMSD (all atoms) 1.2 Å compared to wild type). The first noticeable difference is a small rotation of the PCP domain in relation to the C domain and slight alterations in the PCP interacting regions of the C domain, likely attributable to the R2577G mutation allowing the first helix of the C domain to sit deeper in the acceptor channel (**SI Figure S7**).[5] The major difference, however, is the positioning of the PPant moiety, which now fully extends thought the acceptor channel into the active site (Fig. 4B, **SI Figure S8**) in a similar way to that seen in the ObiF1, SrfA-C and AB3403 structures.[8,10,12] This observation supports the hypothesis that R2577 acts to control substrate access to the active site of the C domain. One possibility is that this process operates by charge repulsion: when an aminoacyl-PPant approaches the acceptor channel, the ammonium group of the substrate triggers the rotation of the Arg side chain due to charge repulsion, which opens the channel, allowing the aminoacyl-PPant to enter it. This would explain our inability to crystallize the wild type PCP_2-C_3 construct loaded with PPant derivatives lacking an amino group (such as propionyl and propan-1,3-dioyl,[33] data not shown), due to interactions that interfere with crystallization when the substrate is not bound in the acceptor channel of the C domain. To further explore this mechanism, we next turned to the characterization of the PCP_2-C_3 construct with an aminoacyl group appended to the PPant thiol group.

Structure of the amino acid acceptor bound substrate. To append the glycyl substrate of module 3 to the PCP_2 domain, we attempted to load the apo-PCP_2C_3 didomain using Sfp and the CoA thioester of glycine. Crystals in the same space group were readily obtained using the same method as for the two previously described structures. Somewhat surprisingly, in this structure it was clear that the electron density

corresponding to the PPant did not sit in the acceptor channel but rather followed the same path as the substrate-free PPant, appearing to be repelled by R2577. However, upon refinement it became clear that the glycyl thioester had been hydrolyzed during crystallization. This forced us to explore alternatives to thioester-tethered amino acids, and we chose to use an analog of the aminoacyl-CoA with a thioether in place of the reactive thioester. This results in a non-hydrolyzable substrate analogue that is still tethered to the PPant via a C-S bond and has a very similar structure to the real substrate (**SI Figure S9**), circumventing issues encountered with other stabilization strategies.[34] To obtain crystals of the PCP_2-C_3 construct with this substrate analogue (hereafter referred to as Gly_{stab}) bound, we again used Sfp to attach PPant-Gly_{stab} to the PCP domain. This construct was then crystallized as previously, resulting in diffraction to a resolution of 1.9 Å (**SI Table S1**).

The overall structure of the Gly_{stab}-loaded PCP_2-C_3 construct was highly similar to the *holo*-PCP_2C_3 construct (572/532 $Å^2$ buried surface area (chain A/B) excluding PPant). In the Gly_{stab} structure, however, the density for the PPant extends through the acceptor channel of the C domain into the active site, as observed in the structure of the R2577G mutant (Fig. 4C-D). R2577 now forms specific interactions with two of the carbonyl oxygen atoms in the Ppant arm (3.7 Å and 3.8 Å), likely acting as a ratchet to hold the Ppant arm (and substrate) in the correct position until after peptide bond formation has occurred (**SI Figure S10**). The PPant-Gly_{stab} extends completely into the active site (Fig. 5A), with the terminal amine of Gly_{stab} stabilized by hydrogen-bond interactions (Fig. 5B). Of particular interest, given the lack of clarity over the role of the active site histidine in the H**H**xxxDE motif, is its close proximity (3.6 Å) to the amino group of the Gly_{stab} moiety. An ordered water molecule also sits close (2.9 Å) to this amino group, where it likely forms a hydrogen bond. By modelling the reaction with density functional theory (Figs. 5C, see Discussion), we predict that N-C bond formation likely precedes N deprotonation and a distinct zwitterionic (oxyanion/ammonium) intermediate is formed (Fig. 5D). This is reminiscent of amide bond formation via reaction of an ester or anhydride with an amine in solution, which is known to occur via a similar mechanism. A significant energy barrier is observed for proton transfer from the zwitterionic intermediate to the imidazole group of the active site histidine residue, suggesting the mechanism of peptide bond formation in C domains relies on specific base catalysis. This may explain why the mutation of this central histidine residue does not completely abolish activity in some C domains, as an active site water molecule could instead play the role of an alternate specific base. The calculations show that the formation of at least one hydrogen bond to the oxyanion is key to stabilizing the zwitterionic intermediate. We also observed the close interaction of the atypical E residue in the HHxxxDE motif (which is typically a Gly in most C-domains) with the nitrogen atom of Gly_{stab} (2.6 Å). It is important to note that Gly_{stab} sits in a different position to the aminoacyl mimic in a previous model of a C domain bound to the acceptor substrate – in these structures the aminoacyl mimic does not enter into the active site as far as observed in our Gly_{Stab}-PCP_2-C_3 complex.[11]

Exploring C domain activity and specificity of the PCP_2-C_3 construct. To test the activity and selectivity of the C domain, as well as the effect of mutating key residues, we first needed to generate an activity

assay for the C domain using the PCP_2-C_3 construct and downstream PCP_3 domain. Given that the interaction between PCP and C domains is weak and transient in nature,[26] we first validated the importance of this restraint in an assay using separately isolated PCP_2-C_3 (loaded with a synthetic dihydroxybenzoic acid (DHB)-D-Arg-Gly donor substrate) and PCP_3-Gly constructs. This experiment revealed no elongation when these constructs were incubated together. Thus, we turned to the use of a fused PCP_2-C_3-PCP_3 construct, albeit one in which the PCP-constructs could be separately loaded with substrates prior to generation of the fused complex (Fig. 6A). To accomplish this, we cloned the donor PCP_2-C_3 construct with a C-terminal SpyCatcher domain and the acceptor PCP_3 with an N-terminal SpyTag peptide.[35] This system allows for the separate loading of the substrates on the PCP domain of each construct using Sfp and synthetic CoA substrates whilst also allowing the reconstitution of the NRPS assembly line.

Using this experimental setup, we confirmed that the condensation reaction was performed as expected, with high levels of conversion of the canonical donor DHB-D-Arg-Gly tripeptide into the Gly-extended tetrapeptide, as determined by high-resolution LC-MS/MS experiments (Fig. 6B). Next, we tested a simplified benzoic acid (BA)-D-Arg-Gly donor substrate in these assays, which showed acceptable levels of conversion (61%) and hence we retained this simplified substrate for all subsequent assays. With a functional condensation assay in hand, we first could verify that the stabilized Gly_{stab} acceptor substrate was a functional mimic of Gly in this C domain (**SI Figure S11**) using intact protein MS together with PPant ejection (see Methods). With confidence that the Gly_{stab} structure represents a functional acceptor substrate-bound C domain state, we then set out to investigate the effect that mutating key residues had on the condensation activity. Firstly, we confirmed that the R2577G mutant C domain retained activity (with Gly), although this was reduced compared to the wildtype C domain (32%), possibly due to the loss of stabilizing interactions with the PPant arm (Fig. 6C, **SI Figure S10**). We next generated an active site H2697Q mutant and determined that H2697 is indeed essential for activity with this C domain, as the mutant only retains ~ 1% of the WT activity with Gly as the acceptor substrate (Fig. 6C).

In addition to Gly and Gly_{stab}, we found that C_3 could also accept PPant-linked L-Ala and L-Leu as substrates, with 99% and 75% conversion levels, respectively (Fig. 6C). In contrast, PPant-linked L-Phe was a poor substrate, with minimal (6%) levels of conversion. In order to rationalize these differences, we analyzed the structures and performed molecular docking. First, assuming that the position of Gly_{stab} in our Gly_{Stab}-PCP_2-C_3 complex represents that catalytically-competent conformation, and that alternate amino acid acceptor substrates must bind in a way that positions the terminal amine group in a similar position, we identified several residues in the central cavity that would likely interact with the side chain of an alternate acceptor substrate. In particular, the side chains of M2917, S2919, Q2921, P2941 and E2950 could contribute a putative side chain binding pocket for this C-domain, in a manner reminiscent of A-domains (Fig. 5B). Molecular docking revealed that sidechains of L-Ala and L-Leu could be accommodated by the active site cavity's side-chain binding pocket and had top scoring poses that positioned the terminal amine towards the catalytic residues (although the L-Leu pose was slightly strained, **SI Figure S12**). In contrast, the bulky side chain of L-Phe could only be accommodated within

the central cavity in poses that positioned the terminal amino acid amine away from the catalytic histidine and that would not be compatible with catalysis (**SI Figure S12**). Analysis of the putative pocket residues (M2917, S2919, Q2921, P2941 and E2950) compared to the reported activity of the downstream A-domain did not reveal any correlation between acceptor substrate and these possible “pocket” residues (Spearman's rho: -0.05), indicating the lack of a C-domain side chain binding pocket and hence “C domain code” comparable to those found with A domains (**SI Figure S13**).[25,36] Our results do however indicate that alterations in the C domain active site can lead to changes in selectivity, and hence we turned to further analysis of the residues within the active site motif.

Although most C domains contain a canonical HHxxxDG motif,[37] the C_3 domain from fuscachelin NRPS features an unusual HHxxxD**E** variant. We hypothesized that, in absence of a side chain in the acceptor substrate (Gly) to position the acceptor substrate, the role of this glutamate (E2702) could be to stabilize and orient the acceptor substrate amine group to ensure an efficient nucleophilic attack of the donor substrate thioester. Indeed, an analysis of C domains where their acceptor substrates are known demonstrated that there is a higher proportion of modified motifs where the acceptor substrate is small as opposed to traditional HHxxxDG containing C domains (**SI Figure S14**). To test this hypothesis, we mutated this glutamate to its canonical glycine residue (E2702G) and performed condensation reactions with Gly as the acceptor substrate. As expected, the condensation level with Gly as the acceptor substrate was reduced by almost half (61–35%) when compared to the WT, demonstrating the non-essential, although beneficial role of this glutamate residue. Interestingly, while the E2702G mutation had reduced activity with the Gly acceptor substrate, this substitution improved the activity for PPant-linked L-Leu from 75–92% (Fig. 6C). This result indicates that the E2702 residue can play a particularly important role in supporting condensation reactions involving Gly as an acceptor substrate, but may be detrimental for other acceptor substrates. Molecular docking of the Gly-PPant and Gly_{stab}-PPant into a model of the E2702G C_3 mutant reveals how the removal of the glutamic acid results in substrate poses that are unlikely to be compatible with catalysis, with the terminal amine of the substrates instead interacting with Glu2950 (**SI Figure S15**).

[1] Superscript indicates the stereochemistry of the C-terminal residue of the donor substrate, subscript indicates the stereochemistry of the acceptor substrate

Discussion

Non-ribosomal peptide synthetases are widely recognized for their impressive selectivity in assembling specific peptide products. While the role of the A domain in substrate selection is clear, the possible role of C domains as a second selectivity filter during peptide assembly has been less well defined. Early studies suggested C domains may show selectivity towards their acceptor substrates,[36] but more recent work has questioned this.[25]

The structural characterization and bioinformatics analysis we have performed of PCP-bound acceptor complexes in this work shows no general correlation between the size or chemical nature of the acceptor

amino acid side chain and potential side chain binding residues in the C domain. Whilst C domain selectivity has recently been characterized in glycopeptide antibiotic biosynthesis,[21] there the mechanism rather acts to ensure that important modifications of the PCP-bound aminoacyl thioester are performed prior to condensation. Whilst some selectivity for the amino acid substrate is seen here, for example in the low conversion (albeit still present) of L-Phe, this appears likely to be due to the significant difference between the small, flexible Gly substrate and L-Phe, with its large, rigid side chain. The influence of the atypical HHxxxDE motif of this C-domain is also seen on lower levels of acceptance of larger amino acids (such as Leu), which can be released upon conversion of the motif into the typical HHxxxDG sequence. This demonstrates the versatile nature of C domains for tolerating active site modifications, some of which can play important additional roles in supporting catalysis.[24]

Within the active site, the amino group of the aminoacyl acceptor lies close to the central histidine residue, with calculations suggesting that this residue could indeed act as a base to deprotonate the zwitterioinic intermediate. Further characterization of the PCP-C complex shows that the PCP binding site of the C domain is, as anticipated, dominated by hydrophobic interactions and is one that is relatively flexible with regards to the PCP domain.[26] Access of the PPant arm to the C domain active site appears to be gated by R2577, which repels the unmodified PPant arm (or neutral/negatively charged substrates) in favor of the aminoacyl-PPant. Whilst this residue is largely conserved in $^{L}C_{L}$ domains, it is typically Gly or other small residues in $^{D}C_{L}$ domains, which we have confirmed allows the unmodified PPant into the C-domain active site. One hypothesis for the role of this residue would be to prevent the unwanted “pass-through” of donor substrates without elongation (e.g. from PCP_2 to PCP_3). Examples of NRPS-dependent pathways in which CP-bound substrate transfer could occur reveals that the C domains implicated bear the Arg to (Gly/small) amino acid mutation (e.g. burkholdac biosynthesis),[38] which provides some support for this hypothesis. For $^{D}C_{L}$ domains, mutation of this Arg residue could be a requirement due to the need for E domain-catalyzed inversion of stereochemistry prior to chain elongation, as we note that the Arg to (Gly/small) mutation generally appears to be somewhat deleterious to peptide conversion levels, possibly due to a lack of interactions between the Arg and PPant arm in these C-domains. We anticipate that the structural snapshots presented here will pave the way for studies to probe the roles of this Arg residue as well as other active site residues in C domain catalysis, which is important due to the ever-increasing roles of C-type domains in non-ribosomal peptide biosynthesis.

Declarations

Competing Interests

G.L.C. is a co-director of Erebagen Ltd. The other authors declare no competing interests.

Author Contributions

The study was designed by T.I and M.J.C. All cloning and protein purification was performed by T.I. and Y.T.C.H. Structural analysis was performed by T.I., Y.T.C.H. and M.J.C. with insightful contributions from G.L.C. and J.A.K. Chemical synthesis was performed by Y.T.C.H. and turnovers results were analyzed by Y.T.C.H. and D.L.S., with M.T. assisting with analysis of HRMS experiments. HRMS and protein MS measurements were performed by D.L.S., R.J.A.G. and R.B.S. Molecular docking and molecular dynamics simulations were performed and analyzed by J.A.K. and C.J.J. Bioinformatics and correlation analyses were performed by A.G. and N.Z. Computational analysis was performed by K.H.C. and E.H.K. The manuscript was written by T.I., Y.T.C.H and M.J.C., with input from the other authors.

Acknowledgements

J. Yin (University of Chicago) for the R4-4 Sfp expression plasmid; M. Kaniusaite (Monash) for assistance with cloning; T. Harshegyi, L. Scully and S. Stamatis (Monash) for assistance with protein purification; D. Maksel & G. Kong (MMCF, Monash) for assistance with crystal screening experiments. This research was undertaken on the MX1 and MX2 beamlines at the Australian Synchrotron, part of ANSTO, and made use of the Australian Cancer Research Foundation (ACRF) detector. We would like to thank the beamline scientists at the Australian Synchrotron for their support during data collection. Computational resources were provided by the National Facility of the Australian National Computational Infrastructure through the National Computational Merit Allocation Scheme and by the University of Queensland Research Computing Centre. This work was supported by Monash University, EMBL Australia, the Australian Research Council (Discovery Project DP190101272 and DP180103047) and the National Health and Medical Research Council (APP1140619 to M.J.C.). T.I. is grateful for the support of the CASS foundation (grant #8583). A.G. is grateful for the support of the Deutsche Forschungsgemeinschaft (DFG; Project ID # 398967434-TRR 261). This research was conducted by the Australian Research Council Centre of Excellence for Innovations in Peptide and Protein Science (CE200100012) and funded by the Australian Government.

References

1. Süssmuth, R. D. & Mainz, A. Nonribosomal Peptide Synthesis—Principles and Prospects. *Angew Chem Int Ed* **56**, 3770–3821, (2017).
2. Walsh, C. T., O'Brien, R. V. & Khosla, C. Nonproteinogenic Amino Acid Building Blocks for Nonribosomal Peptide and Hybrid Polyketide Scaffolds. *Angew. Chem. Int. Ed.* **52**, 7098–7124, (2013).
3. Bloudoff, K. & Schmeing, T. M. Structural and functional aspects of the nonribosomal peptide synthetase condensation domain superfamily: discovery, dissection and diversity. *Biochim. Biophys. Acta* **1865**, 1587–1604, (2017).
4. Keating, T. A., Marshall, C. G., Walsh, C. T. & Keating, A. E. The structure of VibH represents nonribosomal peptide synthetase condensation, cyclization and epimerization domains. *Nat. Struct.*

Mol. Biol. **9**, 522–526, (2002).

5. Tan, K. *et al.* Structures of teixobactin-producing nonribosomal peptide synthetase condensation and adenylation domains. *Curr. Res. Struct. Biol.* **2**, 14–24, (2020).
6. Wang, L., Yuan, M. & Zheng, J. Crystal structure of the condensation domain from lovastatin polyketide synthase. *Synthetic and Systems Biotechnology* **4**, 10–15, (2019).
7. Reimer, J. M. *et al.* Structures of a dimodular nonribosomal peptide synthetase reveal conformational flexibility. *Science* **366**, eaaw4388, (2019).
8. Kreitler, D. F., Gemmell, E. M., Schaffer, J. E., Wencewicz, T. A. & Gulick, A. M. The structural basis of N-acyl-α-amino-β-lactone formation catalyzed by a nonribosomal peptide synthetase. *Nature Commun.* **10**, 3432, (2019).
9. Kosol, S. *et al.* Structural basis for chain release from the enacyloxin polyketide synthase. *Nature Chem.* **11**, 913–923, (2019).
10. Drake, E. J. *et al.* Structures of two distinct conformations of holo-non-ribosomal peptide synthetases. *Nature* **529**, 235–238, (2016).
11. Bloudoff, K., Alonzo, Diego A. & Schmeing, T. M. Chemical Probes Allow Structural Insight into the Condensation Reaction of Nonribosomal Peptide Synthetases. *Cell Chem. Biol.* **23**, 331–339, (2016).
12. Tanovic, A., Samel, S. A., Essen, L.-O. & Marahiel, M. A. Crystal Structure of the Termination Module of a Nonribosomal Peptide Synthetase. *Science* **321**, 659–663, (2008).
13. Tarry, M. J., Haque, A. S., Bui, K. H. & Schmeing, T. M. X-Ray Crystallography and Electron Microscopy of Cross- and Multi-Module Nonribosomal Peptide Synthetase Proteins Reveal a Flexible Architecture. *Structure* **25**, 783–793.e784, (2017).
14. Zhang, J. *et al.* Structural basis of nonribosomal peptide macrocyclization in fungi. *Nature Chem. Biol.* **12**, 1001–1003, (2016).
15. Bloudoff, K., Rodionov, D. & Schmeing, T. M. Crystal Structures of the First Condensation Domain of CDA Synthetase Suggest Conformational Changes during the Synthetic Cycle of Nonribosomal Peptide Synthetases. *J. Mol. Biol.* **425**, 3137–3150, (2013).
16. Samel, S. A., Schoenafinger, G., Knappe, T. A., Marahiel, M. A. & Essen, L.-O. Structural and Functional Insights into a Peptide Bond-Forming Bidomain from a Nonribosomal Peptide Synthetase. *Structure* **15**, 781–792, (2007).
17. Bozhüyük, K. A. J. *et al.* Modification and de novo design of non-ribosomal peptide synthetases using specific assembly points within condensation domains. *Nature Chem.* **11**, 653–661, (2019).
18. Niquille, D. L. *et al.* Nonribosomal biosynthesis of backbone-modified peptides. *Nature Chem.* **10**, 282, (2017).
19. Kaniusaite, M., Goode, R. J. A., Tailhades, J., Schittenhelm, R. B. & Cryle, M. J. Exploring modular reengineering strategies to redesign the teicoplanin non-ribosomal peptide synthetase. *Chem. Sci.* **11**, 9443–9458, (2020).

20. Reitz, Z. L., Hardy, C. D., Suk, J., Bouvet, J. & Butler, A. Genomic analysis of siderophore β-hydroxylases reveals divergent stereocontrol and expands the condensation domain family. *Proc. Natl. Acad. Sci. USA*, 201903161, (2019).
21. Kaniusaite, M. *et al.* A proof-reading mechanism for non-proteinogenic amino acid incorporation into glycopeptide antibiotics. *Chem. Sci.* **10**, 9466–9482, (2019).
22. Patteson, J. B., Dunn, Z. D. & Li, B. In Vitro Biosynthesis of the Nonproteinogenic Amino Acid Methoxyvinylglycine. *Angew. Chem. Int. Ed.* **57**, 6780–6785, (2018).
23. Haslinger, K., Peschke, M., Brieke, C., Maximowitsch, E. & Cryle, M. J. X-domain of peptide synthetases recruits oxygenases crucial for glycopeptide biosynthesis. *Nature* **521**, 105–109, (2015).
24. Gaudelli, N. M., Long, D. H. & Townsend, C. A. beta-Lactam formation by a non-ribosomal peptide synthetase during antibiotic biosynthesis. *Nature* **520**, 383–387, (2015).
25. Calcott, M. J., Owen, J. G. & Ackerley, D. F. Efficient rational modification of non-ribosomal peptides by adenylation domain substitution. *Nature Commun.* **11**, 4554, (2020).
26. Izoré, T. & Cryle, M. J. The many faces and important roles of protein–protein interactions during non-ribosomal peptide synthesis. *Nat. Prod. Rep.* **35**, 1120–1139, (2018).
27. Dehling, E., Rüschenbaum, J., Diecker, J., Dörner, W. & Mootz, H. D. Photo-crosslink analysis in nonribosomal peptide synthetases reveals aberrant gel migration of branched crosslink isomers and spatial proximity between non-neighboring domains. *Chem. Sci.*, (2020).
28. Alfermann, J. *et al.* FRET monitoring of a nonribosomal peptide synthetase. *Nature Chem. Biol.* **13**, 1009–1015, (2017).
29. Reimer, J. M., Aloise, M. N., Harrison, P. M. & Schmeing, T. M. Synthetic cycle of the initiation module of a formylating nonribosomal peptide synthetase. *Nature* **529**, 239–242, (2016).
30. Dimise, E. J., Widboom, P. F. & Bruner, S. D. Structure elucidation and biosynthesis of fuscachelins, peptide siderophores from the moderate thermophile *Thermobifida fusca*. *Proc. Natl. Acad. Sci. USA* **105**, 15311–15316, (2008).
31. Owen, J. G., Robins, K. J., Parachin, N. S. & Ackerley, D. F. A functional screen for recovery of 4'-phosphopantetheinyl transferase and associated natural product biosynthesis genes from metagenome libraries. *Environ. Microbiol.* **14**, 1198–1209, (2012).
32. Sunbul, M., Marshall, N. J., Zou, Y., Zhang, K. & Yin, J. Catalytic Turnover-Based Phage Selection for Engineering the Substrate Specificity of Sfp Phosphopantetheinyl Transferase. *J. Mol. Biol.* **387**, 883–898, (2009).
33. Izoré, T. *et al. Drosophila melanogaster* nonribosomal peptide synthetase Ebony encodes an atypical condensation domain. *Proc. Natl. Acad. Sci. USA* **116**, 2913–2918, (2019).
34. Sztain, T. *et al.* Modifying the Thioester Linkage Affects the Structure of the Acyl Carrier Protein. *Angew. Chem. Int. Ed.* **58**, 10888–10892, (2019).
35. Zakeri, B. *et al.* Peptide tag forming a rapid covalent bond to a protein, through engineering a bacterial adhesin. *Proc. Natl. Acad. Sci. USA* **109**, E690-E697, (2012).

36. Belshaw, P. J., Walsh, C. T. & Stachelhaus, T. Aminoacyl-CoAs as Probes of Condensation Domain Selectivity in Nonribosomal Peptide Synthesis. *Science* **284**, 486–489, (1999).
37. Bergendahl, V., Linne, U. & Marahiel, M. A. Mutational analysis of the C-domain in nonribosomal peptide synthesis. *Eur. J. Biochem.* **269**, 620–629, (2002).
38. Ho, Y. T. C. *et al.* Novel chemical probes for the investigation of nonribosomal peptide assembly. *Chem. Commun.* **53**, 7088–7091, (2017).
39. Biggins, J. B., Gleber, C. D. & Brady, S. F. Acyldepsipeptide HDAC Inhibitor Production Induced in Burkholderia thailandensis. *Org. Lett.* **13**, 1536–1539, (2011).

Figures

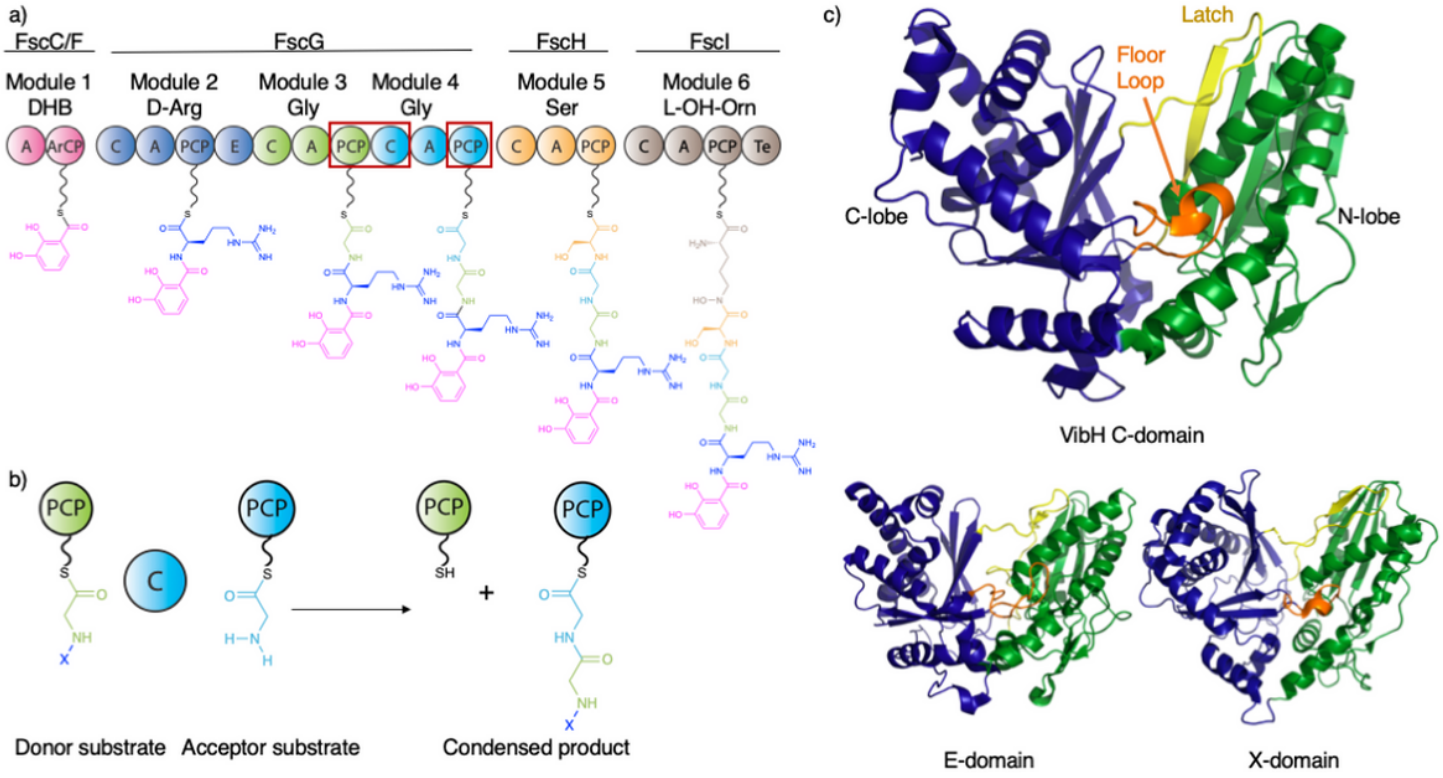

Figure 1

Non-ribosomal peptide biosynthesis and structures of C-type domains. a) Scheme representing the biosynthesis of a linear precursor of fuscachelin A; the domains structurally characterized in this manuscript are indicated by red boxes. b) Condensation domains catalyze peptide bond formation most commonly between thioester intermediates bound to adjacent PCP domains; for mechanistic discussion see Supplementary Information. c) Top: Crystal structure of an archetypal C-domain (VibH from vibriobactin biosynthesis, PDB ID: 1L5A); Bottom left: crystal structure of an epimerization domain from tyrocidine biosynthesis (PDB ID: 2XHG); Bottom right: crystal structure of the cytochrome P450 recruitment (X)-domain from teicoplanin biosynthesis (PDB ID: 4TX2). These domains are all comprised

of a V-shaped pseudo-dimer of chloramphenicol acetyl transferase (CAT) domains (colored green and blue), with crossover regions including the latch (light green) and floor loop (orange). A – adenylation domain; DHB – 2,3-dihydroxybenzoic acid; ArCP – acyl carrier protein; C – condensation domain; E – epimerization domain; PCP – peptidyl carrier protein; Te – thioesterase domain; PPant moieties shown as undulated lines.

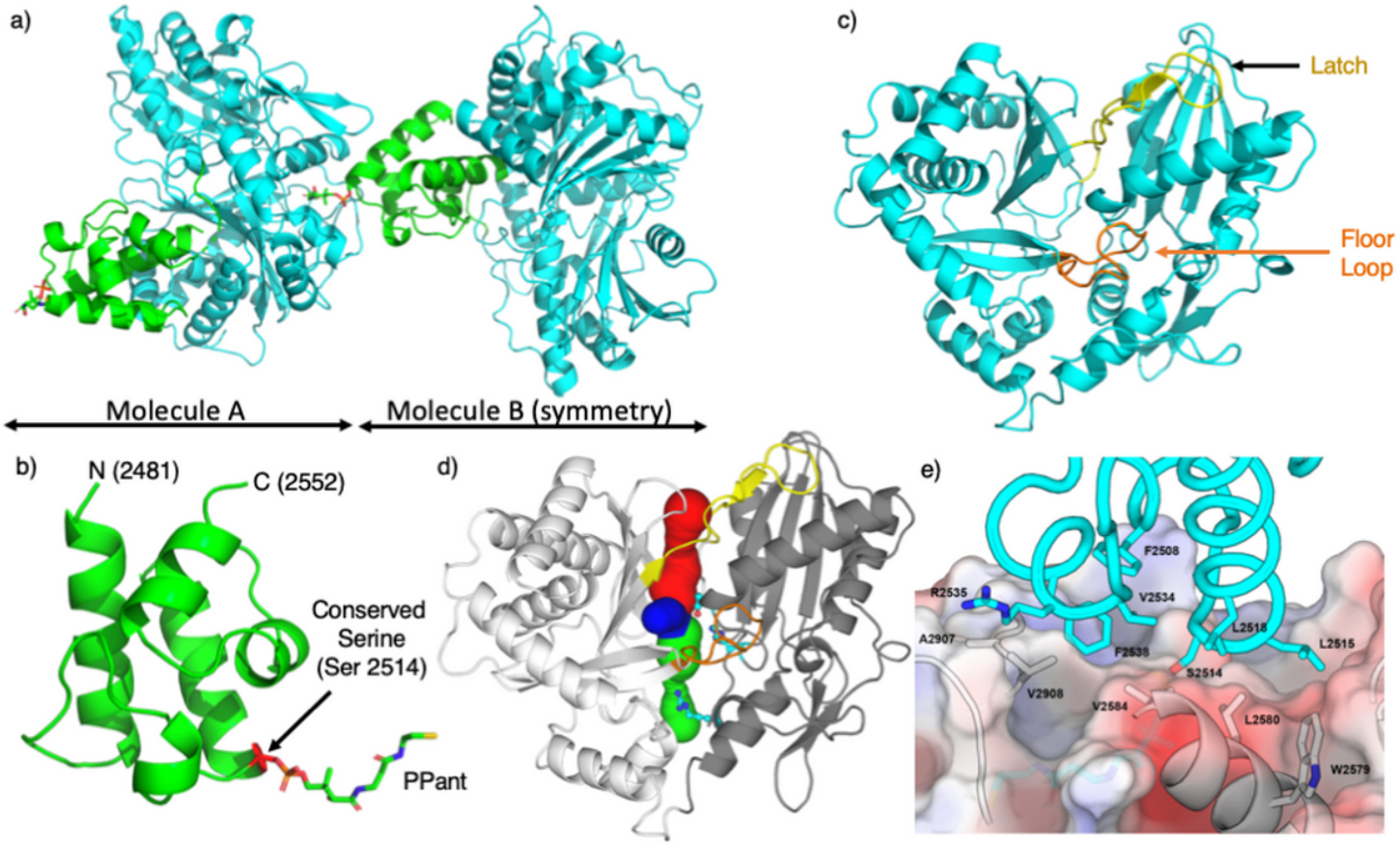

Figure 2

Overview of the structure of the PCP2-C3 didomain from fuscachelin biosynthesis. a) Crystal structure of the PCP2-C3 didomain showing two chains, with the PCP domain docked into the acceptor site of the C domain from another molecule (C domain shown in cyan, PCP shown in green). b) Structure of the PCP2 domain, a 4-helix bundle with an additional small alpha-turn between helices 1 and 2 with the PPant arm bound to Ser2514. c) Structure of the C3 domain, displaying a pseudo-dimer of CAT domains (latch and floor loop regions represented in yellow and orange, respectively); the donor binding site is at the top of the figure and the binding acceptor site is at the bottom of the figure. d) C3 domain showing the donor tunnel (blue), acceptor tunnel (green) and a third tunnel (red) converging on the active site (blue). The tunnel lining residue R2577 and the active site residues E2702 and H2697 are shown as cyan sticks. e) The hydrophobic interface between the PCP2 domain (cyan sticks and ribbon) and C3 domain (surface representation + gray sticks and ribbon).

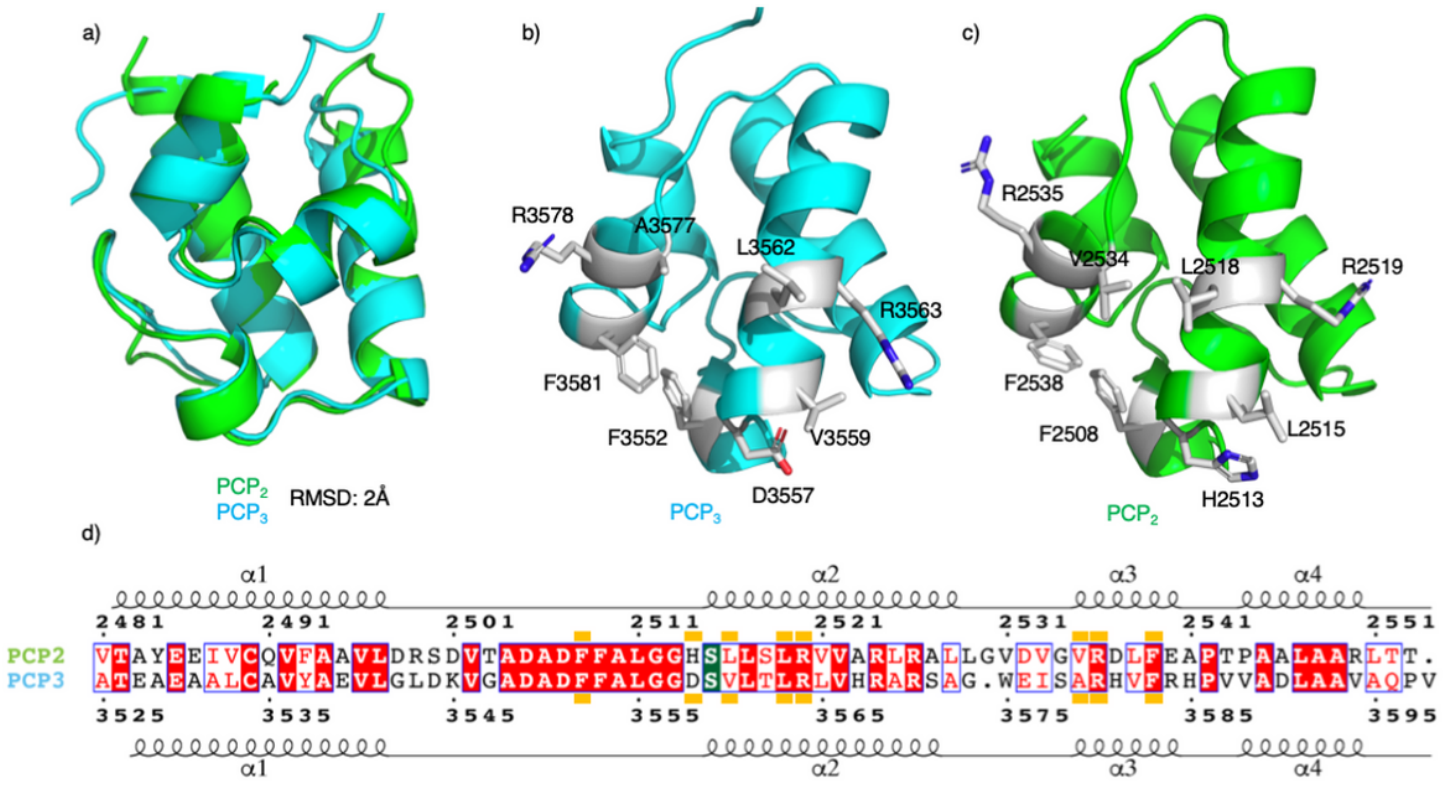

Figure 3

Comparison of PCP2 and PCP3 domains from fuscachelin biosynthesis. a) Structural alignment of PCP2 and PCP3 domains (RMSD 2 Å). b) Crystal structure of the PCP3 domain showing the position of side chains for interaction with C-domain based on PCP2. c) Crystal structure of the PCP2 domain showing side chains interacting with the C-domain. d) Sequence alignment of both PCP2 and PCP3 domains with the C domain interface indicated by orange blocks (conserved residues highlighted in red, similar residues shown in red text).

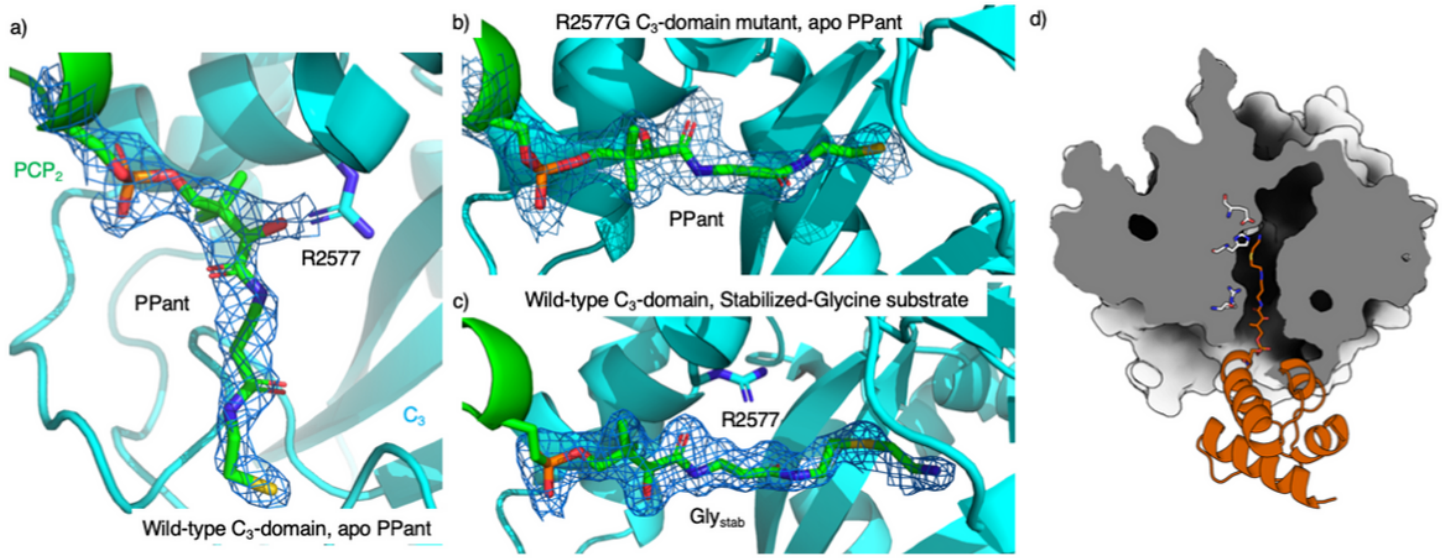

Figure 4

PCP2-C3 interaction surfaces showing the differences in substrate acceptance. a) Structure of WT C3 domain with unloaded PPant, showing the PPant not extending into the C-domain as the side chain of R2577 prevents the PPant accessing the C-domain active site. b) Structure of R2577G C3 domain with an unloaded PPant, showing the PPant fully extended into the C-domain catalytic channel. c) Structure of WT C3 domain where the PPant is loaded with a Glystab substrate, rotated 90 degree anticlockwise compared to panels (a) and (b). Here, PPant-Glystab extends fully into the catalytic channel. d) Cutaway representation of the C domain indicating the path of the Glystab substrate from the PCP domain (shown in orange). All densities shown as 2Fo-Fc maps.

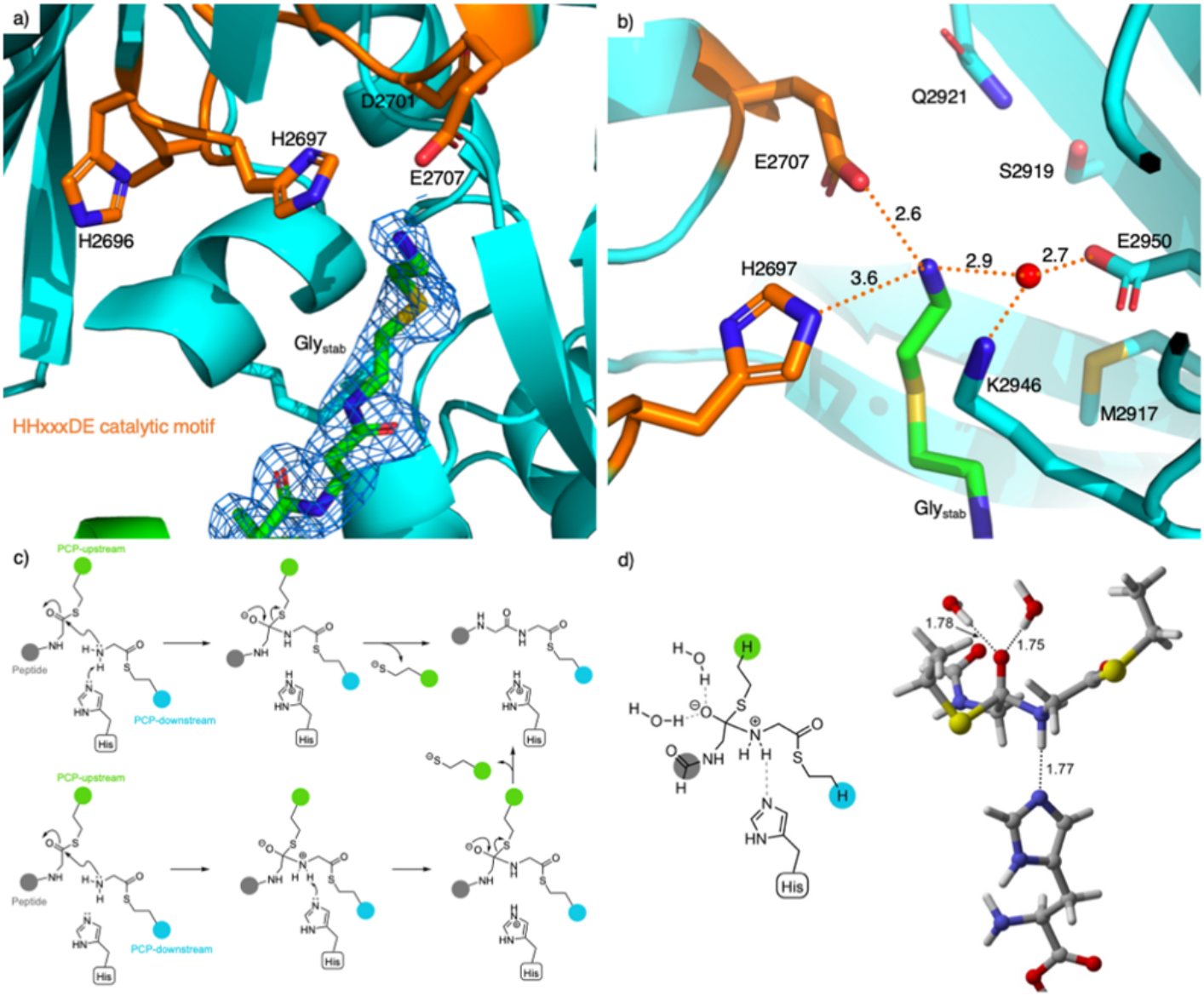

Figure 5

The C3 domain catalytic site showing the docked PPant-Glystab. a) PPant-Glystab substrate extends fully into the active site, approaching the active site HHxxxDE motif (H2696 to E2707); electron density shown as a 2Fo-Fc map. b) The Glystab substrates is stabilized by a network of hydrophilic interactions. Note that residues M2917, S2919, Q2921, P2941 and E2950 are in a position that could potentially

interact with the side chain of alternate acceptor substrates. c) Mechanism of peptide bond formation via concerted N–C bond formation and N-deprotonation (upper) or sequential N–C bond formation and N-deprotonation (lower). d) Zwitterionic intermediate in the sequential N–C bond formation/N-deprotonation pathway, in which the oxyanion is stabilized by two water molecules and the ammonium ion forms a hydrogen bond to histidine.

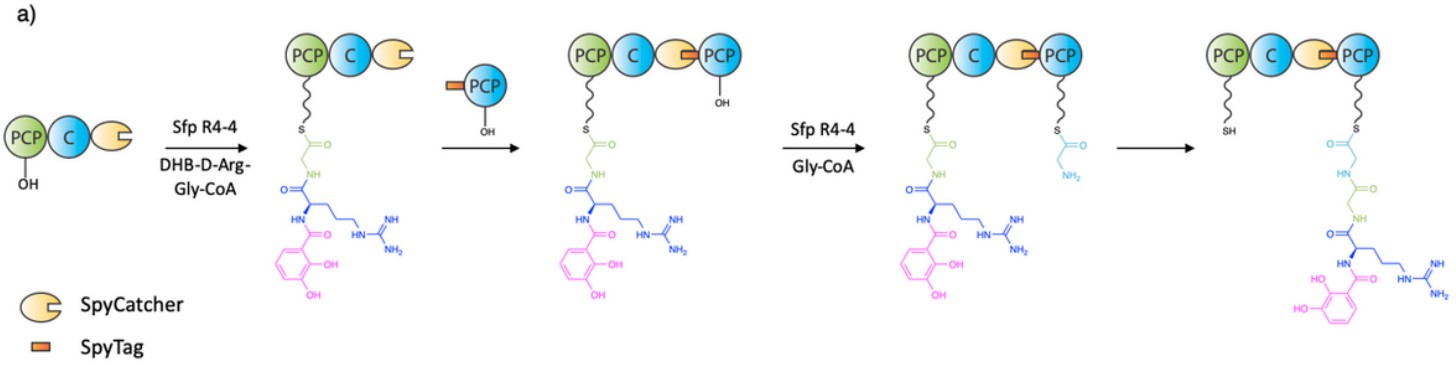

b)

Acceptor substrate	WT	SpyCatcher
Gly	1.4 ± 1.4%	No
Gly	93.9%*	Yes

c)

Acceptor substrate	WT	R2577G	H2697Q	E2702G
Gly	61.4 ± 2.9%	31.9 ± 3.7%	1.2 ± 0.0%	35.4 ± 3.7%
L-Ala	99.3 ± 0.1%	-	-	-
L-Leu	74.6 ± 7.6%	60.1 ± 2.5%#	-	91.7 ± 3.7%
L-Phe	5.8 ± 0.7%	5.9 ± 1.8%	-	2.4 ± 0.4%#

Figure 6

C-domain condensation assays. a) Scheme of the condensation reaction using PCP2C3 SpyCatcher and Spytag-PCP3 constructs. b) Level of tetrapeptide formation demonstrated by the WT C-domain with or without SpyCatcher and SpyTag; the reaction was performed using a DHB-D-Arg-Gly donor substrate and a Gly acceptor substrate. c) Level of tetrapeptide formation by WT and different C-domain mutants using BA-D-Arg-Gly as a donor substrate and different aminoacyl acceptor substrates. All reactions performed in triplicate, unless specifically stated (* single reaction; # duplicate); see Supplementary Information for traces.

Supplementary Files

This is a list of supplementary files associated with this preprint. Click to download.

- 7KVWvalidationreport.pdf
- 7KW0validationreport.pdf
- 7KW2validationreport.pdf
- 7KW3validationreport.pdf
- SupplementaryInformationCryle2020.pdf
- ReportingSummaryCryle.pdf